Combining imaging flow cytometry and machine learning for high-throughput schistocyte quantification: A SVM classifier development and external validation cohort

Julien Demagny,[a,b] Camille Roussel,[c,d,e] Maïlys Le Guyader,[b] Eric Guiheneuf,[b] Véronique Harrivel,[b] Thomas Boyer,[a,b] Momar Diouf,[f] Michaël Dussiot,[e,g] Yohann Demont,[b,1]* and Loïc Garçon [a,b,1]*

[a]Univ. Picardie Jules Verne, HEMATIM UR4666, F80025, Amiens, France
[b]Service d'Hématologie Biologique, CHU Amiens-Picardie, Amiens, France
[c]APHP, Laboratoire d'Hématologie, Hôpital Universitaire Necker-Enfants Malades, Paris, France
[d]Biologie Intégrée du Globule Rouge, INSERM U1134, Université de Paris, Université des Antilles, Paris, France
[e]Laboratoire d'Excellence GR-Ex, Paris, France
[f]Département de biostatistiques, Direction de la Recherche Clinique et de l'Innovation, CHU Amiens-Picardie, Amiens, France
[g]U1163, Laboratoire des mécanismes cellulaires et moléculaires des troubles hématologiques et de leurs implications thérapeutiques, INSERM, Université de Paris, Paris, France

Summary

Background Schistocyte counts are a cornerstone of the diagnosis of thrombotic microangiopathy syndrome (TMA). Their manual quantification is complex and alternative automated methods suffer from pitfalls that limit their use. We report a method combining imaging flow cytometry (IFC) and artificial intelligence for the direct label-free and operator-independent quantification of schistocytes in whole blood.

Methods We used 135,045 IFC images from blood acquisition among 14 patients to extract 188 features with IDEAS® software and 128 features from a convolutional neural network (CNN) with Keras framework in order to train a support vector machine (SVM) blood elements' classifier used for schistocytes quantification.

Finding Keras features showed better accuracy (94.03%, CI: 93.75-94.31%) than ideas features (91.54%, CI: 91.21-91.87%) in recognising whole-blood elements, and together they showed the best accuracy (95.64%, CI: 95.39-95.88%). We obtained an excellent correlation (0.93, CI: 0.90-0.96) between three haematologists and our method on a cohort of 102 patient samples. All patients with schistocytosis (>1% schistocytes) were detected with excellent specificity (91.3%, CI: 82.0-96.7%) and sensitivity (100%, CI: 89.4-100.0%). We confirmed these results with a similar specificity (91.1%, CI: 78.8-97.5%) and sensitivity (100%, CI: 88.1-100.0%) on a validation cohort (n=74) analysed in an independent healthcare centre. Simultaneous analysis of 16 samples in both study centres showed a very good correlation between the 2 imaging flow cytometers (Y=1.001x).

Interpretation We demonstrate that IFC can represent a reliable tool for operator-independent schistocyte quantification with no pre-analytical processing which is of most importance in emergency situations such as TMA.

Funding None.

Keywords: Schistocyte; Imaging flow cytometry; Machine learning; Thrombotic microangiopathy

eBioMedicine 2022;83: 104209
Published online xxx
https://doi.org/10.1016/j.ebiom.2022.104209

*Corresponding authors at: Service d'Hématologie Biologique, CHU Amiens-Picardie, Amiens, France.
E-mail addresses: demont.yohann@chu-amiens.fr (Y. Demont), garcon.loic@chu-amiens.fr (L. Garçon).

[1] Equal contribution.

Research in context

Evidence before the study

We searched PubMed using the search terms "imaging flow cytometry", "learning", "red blood cell morphology", "schistocyte" and associated permutations to find relevant articles until March 2018. Imaging flow cytometry combined with machine learning appears to be a promising tool in haematology, allowing a high input blood cell recognition and quantification. Red blood cell diseases seem to be particularly suitable for this type of approach, especially those that require urgent diagnosis but suffer from a lack of standardisation such as schistocyte identification and count. PubMed search provided preliminary resources and even some methods for the automatic assessment of blood cells morphologies but far from a potential application in routine. As a matter of facts, they confirmed the conclusions of the International Council for Standardisation in Haematology for the need of new tools to allow reliable, high-throughput, and automated quantification of red blood cells.

Added value of this study

We constitute the largest expert-annotated pool of images from blood collection acquired with state-of-the-art imaging flow cytometry available in the literature with as much as 135,000 images. This has permitted us to build an outmost quality classifier capable of discriminating between 29 different categories. The strategy presented in this manuscript allows the acquisition of a large number of blood cells and their identification in few minutes without any pre-processing step. As exemplified with schistocytes, our approach was used to address a clinically relevant question while avoiding expert-recognised pitfalls of current gold standard. It has been applied in two medical centres on more than 100 patients' blood and has led to the categorisation of patients with high amount of schistocytes with remarkable performance.

Implications of all the available evidence

What we have described here should lead to refinement of patient management such as thrombotic microangiopathy where schistocytes elevation is a key point of the diagnosis in emergency context. Finally, our work extends current boiling research in the field of imaging flow cytometry and we clearly believe that it can accompany the future of red blood cells morphologies investigation in clinics.

Introduction

Red blood cell (RBC) morphology is at the front line in the diagnostic process for anaemia, guiding the prescription of second-line tests. The importance of this assessment is underlined by the International Council of Standardisation in Haematology (ICSH) recommendations for the semi-quantitative classification of all RBC shapes using three different grades.[1] Among RBC morphologies, schistocytes are of particular interest. Absent or rare in the blood of healthy patients,[2,3] their presence reflects the mechanical fragmentation of RBCs that can occur in various contexts, mainly related to mechanical obstacles, such as fibrin filaments, high shear stress, or thermal injury.[4] Importantly, their detection is a key point in the diagnosis of thrombotic microangiopathies (TMA), including thrombotic thrombocytopenic purpura (TTP), haemolytic uremic syndrome (HUS), and other situations, such as metastatic cancer, haematopoietic stem-cell transplantation, haemolysis with elevated liver enzymes and low platelet count (HELLP) syndrome, and eclampsia.[5,6] The state of the art in terms of schistocyte quantification is currently based on morphological evaluation of RBCs by the analysis of blood smears after May Grümwald Giemsa coloration.[4,7,8] The International Council for Standardisation in Haematology (ICSH) guidelines defines specific positive morphological criteria and typical RBC shapes (keratocytes, helmet cells, crescents, and triangles) and recommends counting schistocytes among at least 1,000 RBCs[7,8] to significantly improve the standardisation of their quantification. Nonetheless, the schistocyte count is probably among the most important parameters to be automated. Indeed, (i) it is the only RBC morphology that must be quantitatively estimated, given the robust positive predictive value of the 1% cut-off in TMA, which may require immediate clinical management, such as plasma exchange in TTP,[5–9] (ii) such quantification is complex, time-consuming, and requires a well-trained operator, and (iii) reliability of the result depends on the number of cells counted and the quality of the blood smears and is sensitive to inter-observer variability.[10] Progress in the standardisation of this technique has been made by automating the review of blood smears using a digital camera coupled to an artificial neural network. This technology, particularly efficient for white blood cell (WBC) identification and quantification,[11] classifies RBCs according to their size, shape, colour, and inclusion features and provides a semi-quantitative assessment for each.[11,12] Although attractive, it still requires manual post-classification by a trained operator to be sufficiently reliable for diagnosis, especially for the schistocyte count.[13,14] In addition, the accuracy of this approach is highly affected by the quality of the blood smear and its staining.[4,11,15]

Imaging flow cytometry (IFC) is an innovative tool that has the advantage of combining high-throughput technology with morphological analysis in the absence of pre-analytical procedures, which may modify cell shape. Indeed, IFC has proven its ability to identify various RBC anomalies, including sickle cells,[16] intra-erythrocyte malaria,[17] RBC storage lesions,[18,19] and spherocytes.[20] However, the above-mentioned studies

were based on classical IFC procedures, including ad hoc masking and image feature extraction using IDEAS® software.[21] New perspectives have recently been opened by pioneering studies that have introduced artificial intelligence (AI) to the field of IFC,[22] particularly for leucocyte classification[23,24] and the identification of acute lymphoblastic leukaemia.[25] More recently, it was shown that AI combined with IFC can be used to monitor morphological alterations of stored RBC concentrates[26] in addition to efforts undertaken to produce highly reproducible results between laboratories.[27] Here, we aimed to apply these technologies to schistocyte recognition and developed a label-free machine learning-based identification method for RBCs to establish IFC as a reliable method for the direct operator-independent quantification of schistocytes in whole blood, with no pre-analytical processing.

Methods

Samples

All peripheral venous blood samples were collected as part of the regular follow-up of patients in EDTA-K2-anticoaguled tubes (Vacutainer, Becton Dickinson, Sunnyvale, CA, USA). Only the remaining blood in the tubes, after all requested analyses were performed, was used for this study. Blood smears performed prior to IFC acquisition, either manually or using an Advia Autoslide (Siemens Healthcare Diagnostics, Tarrytown, NY) or SP-50 (Sysmex Corporation, Kobe, Japan). Blood smears were stained using May-Grünwald Giemsa.

Ethics

This study followed the French regulations governing non-interventional studies and was approved by the Clinical Research and Innovation Department of hospital CHU Amiens-Picardie and Assistance Publique des Hôpitaux de Paris (APHP) (PI2021_843_0087). As per French legislation, no specific patient consent was required. The analysis of biological samples obtained in the medical care context was considered as non-interventional research (article L1221-1.1 of the French Public Health Code), requiring only the non-opposition of the patient during sampling (article L1211-2 of the French Public Health Code).

Sample size

The sample size cohort was established in order to include approximately 1/3 positive samples and 2/3 negative samples with more than 70 samples per cohort to balance with feasibility, sample availability and accurate assessment of our tool. The samples were selected not consecutively but randomly according to the availability of the samples, the investigators and imaging flow cytometer. Inclusion criteria was schistocyte count requested by physicians and exclusion criteria was sample collected more than 24 hours before acquisition.

Validation cohort

In Amiens hospital, 102 samples (different from the ones used for the training) from 86 patients for whom a schistocyte count was requested by physicians were selected between June 2018 and September 2020. Among them, 33 had > 1% schistocytes as assessed by morphological examination of blood smears, 10 samples had between 0.5 and 1% schistocytes and 59 samples had < 0.5% schistocytes. Schistocytosis aetiology, complete blood count (CBC), haemolysis work-up and history of RBC/platelet/plasma transfusion are indicated in Suppl. Table S1. Schistocytes were enumerated blindly, and without knowledge of the IFC schistocyte

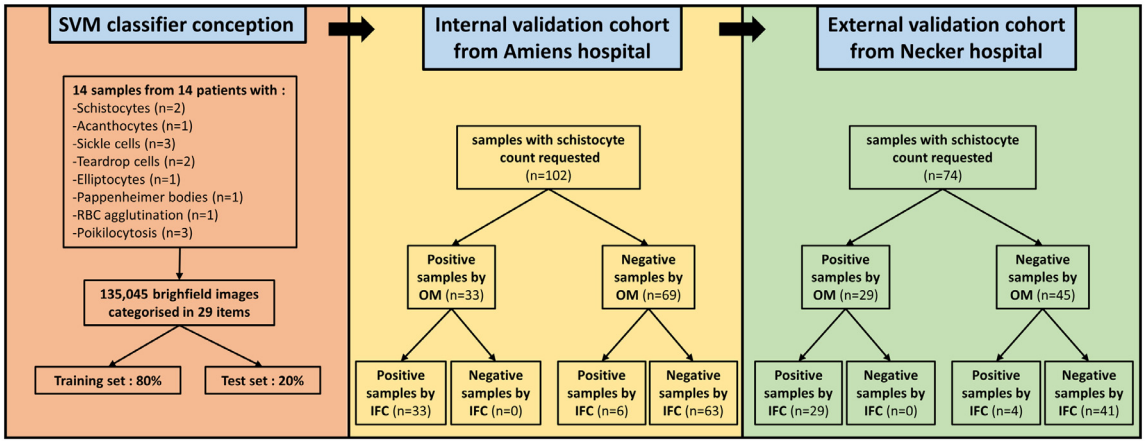

Figure 1. Study flow diagram. Left panel, SVM classifier conception using 14 samples different from the ones used for the internal and external validation cohorts. Middle panel, internal validation cohort (Amiens). Right panel, external validation cohort (Necker). Positive samples as defined by schistocyte count above 1% with OM and 1,92% with IFC. OM: optical microscopy, IFC: imaging flow cytometry.

count, among 1,000 RBCs by three independent well-trained haematologists using an optical microscope (OM) at 1000X magnification according to the Schistocyte Working Group of the ICSH recommendations.[7,8] As a control group, 39 samples from healthy patients with a normal complete blood count and no schistocytosis, as assessed by cytology, were collected.

For the external validation cohort, 74 samples (42 patients) from Necker hospital (APHP, Paris) for whom a schistocyte count was requested were acquired between October 2021 and February 2022. Among them, 29 had more than 1% schistocytes as assessed by morphological examination of blood smears. Schistocytosis aetiology, CBC and haemolysis work-up for each patient are indicated in Suppl. Table S2. Schistocytes were enumerated by laboratory medical staff from Necker hospital. Samples with less than 1% of schistocytes were reported as <1%. A demographic table to compare both cohorts and a study flow diagram to show the disposition of patients in the study is available in Suppl. Table S3 and Figure 1.

IFC acquisition

Samples were diluted 1:50 in 1X calcium and magnesium-free phosphate-buffered saline and 100 µL injected into an ImageStream (IS) X Mark II (Amnis, Luminex, Seattle, WAS, USA). Training and validation sets (Amiens hospital only) were constructed using image files acquired with the brightfield intensity set to 780, 800, and 820 and up to 100,000 events were recorded for each brightfield setting. For the validation cohort comprising samples from Amiens hospital and Necker Hospital, brightfield was acquired on channel 4 with the intensity set to 800, in total, 10,000 objects were captured.

Instrument characteristics

In Amiens CHU, ImageStream (IS) X Mark II was equipped with one camera (Hamamatsu) and 375, 488, 642, and 785 nm excitation lasers. Samples were acquired with INSPIRE software (v200.1.388.0 to v200.1.620.0) and lasers powered at 50, 200, 150, and 0.3 mW, respectively. Channels 1, 4, and 6 were collected at high sensitivity and 60x magnification. In Necker Hospital, ISX was equipped with two cameras (Sarnoff) and 375, 405, 488, 561, 642, and 785 nm excitation lasers. And, samples were acquired at 60x magnification on all channels of the first camera (01 to 06) with INSPIRE software (201.1.0.693) with only 785 nm laser powered at 0.3 mW.

Design of the database corresponding to the training and validation sets

The training and validation sets were constructed from 14 selected samples containing various morphologies of interest observed on blood smears, including schistocytes (n=2), acanthocytes (n=1), sickle cells (n=3), teardrop cells (n=2), elliptocytes (n=1), Pappenheimer bodies (n=1), RBC agglutination (n=1), and anemia/poikilocytosis (n=3). All images from the brightfield channel were extracted and classified to retain the events of interest. All corresponding objects were merged into a single file that was then used for feature extraction. Of note, none of the samples included in the database were used for the validation cohort. The process for the database design and sample analysis is summarised in Suppl. Figure 1.

Feature extraction and modelling

Computations were performed using a 2 x Xeon E5-2620 (total 12 physical cores) analysis station, bought with the IS but upgraded with a NVIDIA GTX1050Ti (4 GB) and extra RAM (total 48 GB), and windows 7 with R and the abind, caret, e1071, keras, IFC, and tensorflow R packages (software versions are provided in Suppl. Table S4). IDEAS® analysis software was used to process the acquired data to generate the so-called ideas features from brightfield images. In total, 188 features were used. Feature-value extraction was highly facilitated by our publicly available IFC package, allowing us to batch extract feature values directly from daf files created by the IDEAS® software. For the so-called keras features, we used a simple convolutional neural network (CNN) consisting of several stacks of convolutional and drop layers. Just before the final softmax multi-class output, we placed a dense layer of 128 units to extract 128 features resulting from the training. The input consisted of 80 square-pixel brightfield images shaped using the abind package to an array of [1, 80, 80, number of events] extracted using the IFC package with clipped object removal and intensity-value ranges normalised to [0, 1] for each single object. The weights of the CNN were adjusted using the R packages keras and tensorflow at the backend without setting tensorflow seed and using the capability of the graphic processing unit (GPU) for a total of 100 epochs, a batch size of 256, and data augmentation (horizontal and vertical image flipping, shearing up to 0.15, zooming range up to 0.15, shifting up to 0.2, and rotating up to 45°) while reserving 20% of each class for the validation step. For CNN training, we used more categories than for the SVM, as certain classes were gathered or selected. After 3.772895 h, we obtained a final accuracy of 0.9055654 for the validation set. The CNN was fitted with callbacks for tensorboard logging, early stopping, and best model checkpoint saving used for keras features extraction. We used the support vector machine (SVM) to build a 29 categories classifier owing to its high performance in classification tasks.[28] All features were centered and scaled against the mean and the standard deviation of the 135,045 brightfield images from 14 patients transformed in features (namely keras and ideas) entering the SVM and the polynomial basis function allowing for

non-linearity was used as kernel. The training dataset consisting of 80% of the 135,045 brightfield images was divided into five equal size subsets (5-folds cross validation) with each combination of four subsets used for models training and the fifth subset for validation. During cross validation, the SVM model parameters from the e1071 package, degrees (the degree of the polynomial kernel) [2, 3], coef0 (constant of kernel formula) [10, 20, 50], cost (penalty for misclassification) [0.1, 1, 5], and γ (function of the deviation of the kernel) [0.0001, 0.001, 0.01] were optimised with grid-searching controlled by the caret package to minimise the negative of multinomial log-likehood (smaller is better) based on the class probabilities in unseen data. After finding the best (degree, coef0, cost, and γ) combination, the whole training dataset was trained again to generate the final classifier. Three SVM models were created, one with the ideas features alone, another one with the keras features alone, and a third with both the ideas and keras features which required 1.187054, 3.65764, and 2.238624 days, respectively under parallel computation. Intensity-based ideas features were transformed with smoothLinLog function from IFC. Missing data that may arise during the process of brightfield image features extraction and SVM classification have been handled so that they do not fall under the decision threshold (DT) used and does not allow for cell identification.

Data

Data from patients were collected and entered by J.D. and C.R. into a computerised database encrypted and ruled by the Clinical Research and Innovation Department of hospital CHU Amiens-Picardie. This computerised database was used for the statistical analysis. Missing data were marked as not available in the Suppl. Tables S1 and S2 and analysis was performed without.

Statistics

Quantitative variables were expressed as mean ± standard deviation or as median [Interquartile range] and qualitative variables were expressed as frequency and percentage. Spearman's rank correlation coefficients (r_s) were used to evaluate the correlation between the percentage of cell counts obtained with IFC and those on blood smears. A random effect-based ANOVA intraclass correlation coefficient was used to evaluate the agreement between hematologists' schistocyte counts.[29] Degree of freedom was estimated according to Shrout et al.[30] Comparison of schistocyte counts between three groups was performed with Kruskal-Wallis test with Dunn's multiple comparisons. Within-run precision was calculated using the coefficient of variation (CV). No allowance for multiplicity has been applied. Discriminative performance of the SVM was assessed by mean of AUC with a 95% CI. Sensitivity, specificity, PPV and NPV were also calculated with 95% CIs. Then, the classifier was further tested in two datasets (Amiens dataset and Paris dataset) with calculation of diagnostic performance indices. Statistical analysis was performed using GraphPad Prism and R. Software version can be found in Suppl. Table S4.

Role of funders

No specific funding.

Results

Expert-based design of RBC morphology identification

To differentiate schistocytes from other elements, we created 29 categories that correspond to either (i) specific RBC types *i.e.* regular RBCs, reticulocytes, echinocytes, ovalocytes, acanthocytes, sickle cells, teardrop cells, elliptocytes, punctae RBCs, micro-spherocytes and schistocytes (including keratocytes, triangles, tricorns, crescents and helmet cells, as recommended by the ICSH), (ii) other cell types *i.e.* white blood cells and platelets, (iii) incidental events and coincident cells *i.e.* RBC aggregates, beads, lysis cells, cells and beads, cells and platelets, cells and white blood cells, cut cells, ghost, hemi-cells, non-singlet beads, non-single RBC, platelet doublets, platelet aggregates and (iv) non front-orientated RBC i.e. orientation shape 1, 2 and 3 (Figure 2 and Suppl. Table S5). Micro-spherocytes were not included in the schistocytes group as they were shown to be an overspreading artefact and subsequently irrelevant here.[7,8,31] Various RBC shapes from the 14 samples selected for the database design were acquired by IFC as described in the Methods section. Images from the brightfield channel were extracted, classified into one of the 29 categories by two independent trained operators or excluded if they did not correspond to any of them. Thus, we created a database containing a set of 135,045 images. The dimensionality reduction-based technique t-SNE showed nice clustering of all categories using keras alone and the combination of ideas+keras features (Figure 3, Suppl. Figure S2 and Suppl. File S1). We split all identified images into two sets.[32,33] A training set, representing 80% of each category, was used to create three prediction models using (i) ideas features, (ii) keras features (iii), or ideas+keras features. A validation set of the remaining 20% of the images was used to evaluate the performance of the modelling. From this test set, we computed confusion matrices to assess the accuracy of each prediction. The overall accuracy (ratio of the number of correctly classified events to the total number of events) was 91.54% (CI: 91.21-91.87) using ideas features, 94.03% (CI: 93.75-94.31%) using keras features, and 95.64% (CI: 95.39-95.88) using ideas +keras features. Individually, the accuracy of the 29 categories ranged from 64.7% to 99.7% using ideas features, 47.1% to 99.7% using keras features, and 76.5%

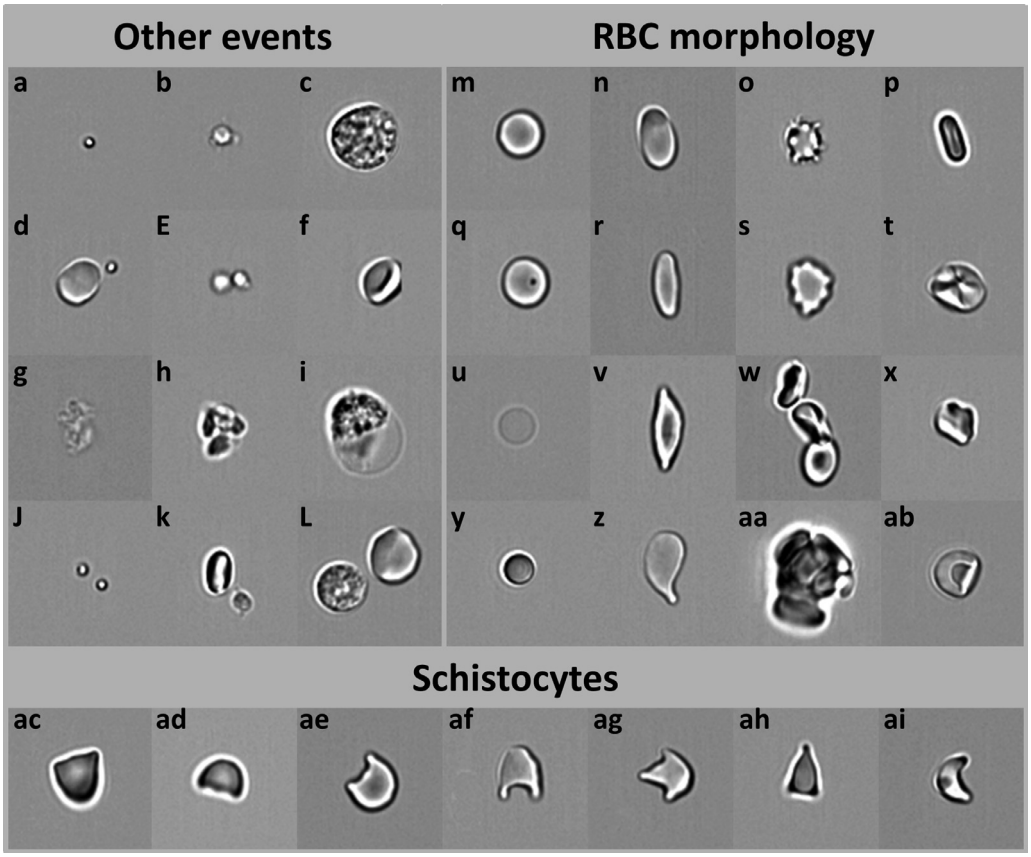

Figure 2. Representative images from the 29 categories of the SVM classifier. Other events (left panel): (a) beads, (b) platelets, (c) white blood cells, (d) cells and beads, (e) platelet doublets, (f) cut cells, (g) lysis cells, (h) platelet aggregates, (i) hemi-cells, (j) non-singlet beads, (k) cells and platelets, (l) cells and white blood cells. RBC morphology (right panel): (m) regular RBC, (n) ovalocytes, (o) acanthocytes, (p) orientation shape 1, (q) punctae RBC, (r) elliptocytes, (s) echinocytes, (t) reticulocytes, (u) ghost-like RBC, (v) sickle cells, (w) non-singlet RBC, (x) orientation shape 3, (y) microspherocytes, (z) teardrop cells, (aa) RBC aggregates, (ab) orientation shape 2. Schistocytes: (ac and ad) helmet cells, (ae and af) keratocytes, (ag) tricorns, (ah) triangles, (ai) crescents.

and 99.7% using both. Focusing on schistocytes, the sensitivity was 75.6%, 86.9%, and 89.1% using the ideas, keras, and ideas+keras features, respectively (Figure 4 and Suppl. Figure S3). Specificity, sensitivity and F1 score are shown in Suppl. Table S6). Overall, these data show better performance for the keras than ideas features in terms of schistocyte recognition and a slight improvement when both features were combined.

Cytological quantification of schistocytes in the validation cohort and optimisation of the correlation between IFC and optical microscopy count

Manual quantification of schistocytes on blood smears was performed by three well-trained haematologists for the 102 samples of the validation cohort from Amiens hospital described in the Methods section. The intra-class correlation coefficient, which measures the degree of agreement between operators, was 0.91 (95% CI: 0.88-0.93), showing excellent inter-observer reliability.[29] Consequently, we used the mean schistocyte count of the three haematologists to evaluate the correlation between the percentage of schistocytes using IFC and OM. The percentage of schistocytes by IFC was defined as the predicted percentage of schistocytes divided by the predicted number of single RBCs (Figure 2 m-o, q-v, x-z, and ab-ai). To optimise this correlation, we computed the class probability of the prediction and applied a threshold on this value, called the decision threshold (DT), for the ease of reading hereunder. Indeed, each time the SVM classified an image, it assigned a probability of its being correctly categorised. We increased specificity by excluding images with an insufficient degree of confidence thanks to the application of a threshold from 0.5 to 0.99 on the maximal probability. The prediction model using ideas features showed a correlation between IFC and OM for the percentage of schistocytes from 0.76 to 0.91, depending on the DT. The correlation ranged from 0.84 to 0.93 using

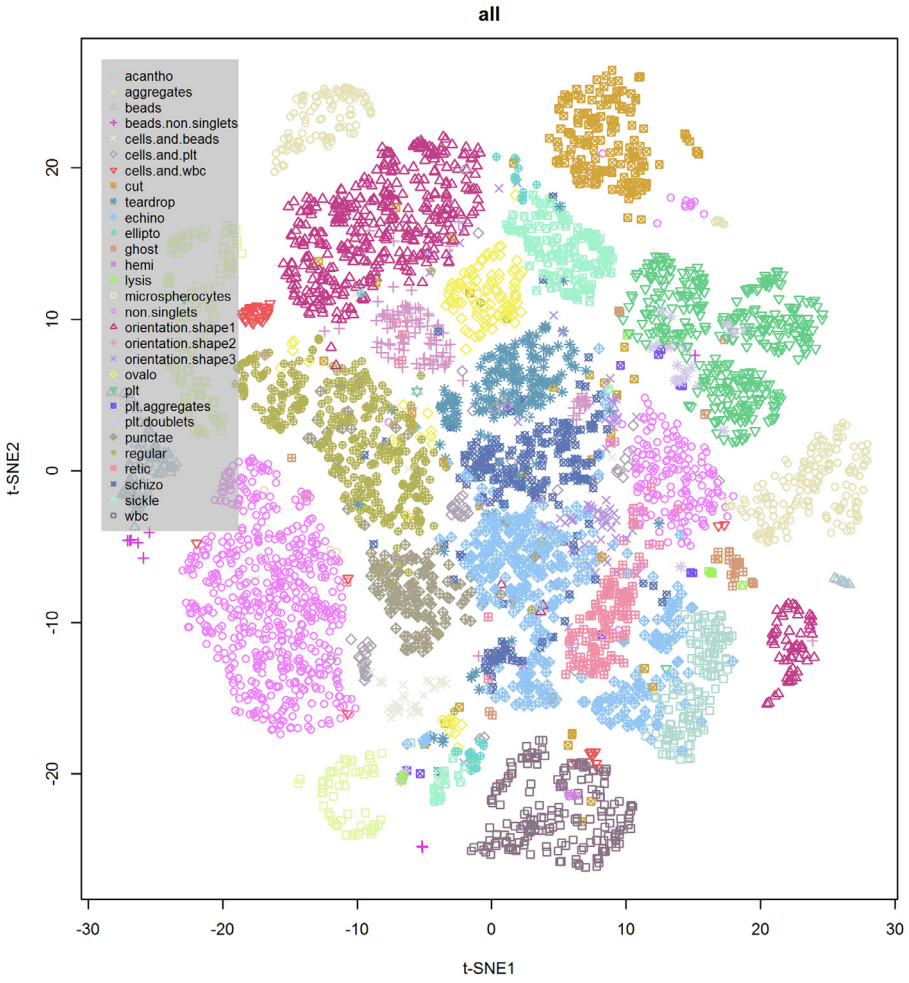

Figure 3. t-SNE plot of the 29 events categorised using ideas+keras features. Each symbol and colour combination refers to a tagged event. The representation was obtained from randomised events (*n*=5000). See in Suppl. File 1 for the three-dimensional visualisation of the t-SNE plot with image embedding.

keras features and 0.89 to 0.93 using ideas+keras features with the same DT (Figure 5a, b, and c). We therefore selected the combined ideas+keras prediction model and a DT of 0.90 for further analysis, as it led to the highest correlation between the haematologists and IFC (mean observer: 0.93; 95% CI: 0.90-0.96, individual observer in Suppl. Figure S4) (Figure 5). At this threshold, the percentage of schistocytes by IFC was evaluated with an average of 3,300 RBCs (95% CI: 3227-3372) (Figure 5d). We used linear regression to determine the conversion rate of the percentage of schistocytes between IFC (Y) and cytology (X) with the equation Y = 1.92X (Figure 6).

IFC as a tool for schistocyte quantification: reference value, within-run precision, dilution linearity, and acquisition time

We also analysed the blood of 39 healthy patients with no significant schistocytosis to determine the reference value for schistocyte quantification by IFC. The median percentage of schistocytes was 0.19% [0.14-0.28 %] and significantly lower than that in the samples (negative samples median: 0.61% [0.35-1.13%], p <0.001; positive samples median: 6.68% [4.15-7.56%], p <0.001; Kruskal-Wallis test with Dunn's multiple comparisons) for which a schistocyte count was requested by physicians (Suppl. Figure S5). We evaluated the within-run precision by performing three successive acquisitions with 88 among the 102 samples used for the validation cohort from Amiens hospital. We observed a good coefficient of variation (CV) whether the samples contained a low or high percentage of schistocytes, as determined by IFC (median CV = 17.7% [10.1-32.1] for samples with < 1% schistocytes and median CV = 6.0% [4.4-9.1] for samples with > 1% schistocytes). These CV values were significantly (p <0.0001, Wilcoxon test) better than those obtained using OM (median CV = 66.4% [23.5–128.6] for samples with < 1% schistocytes and

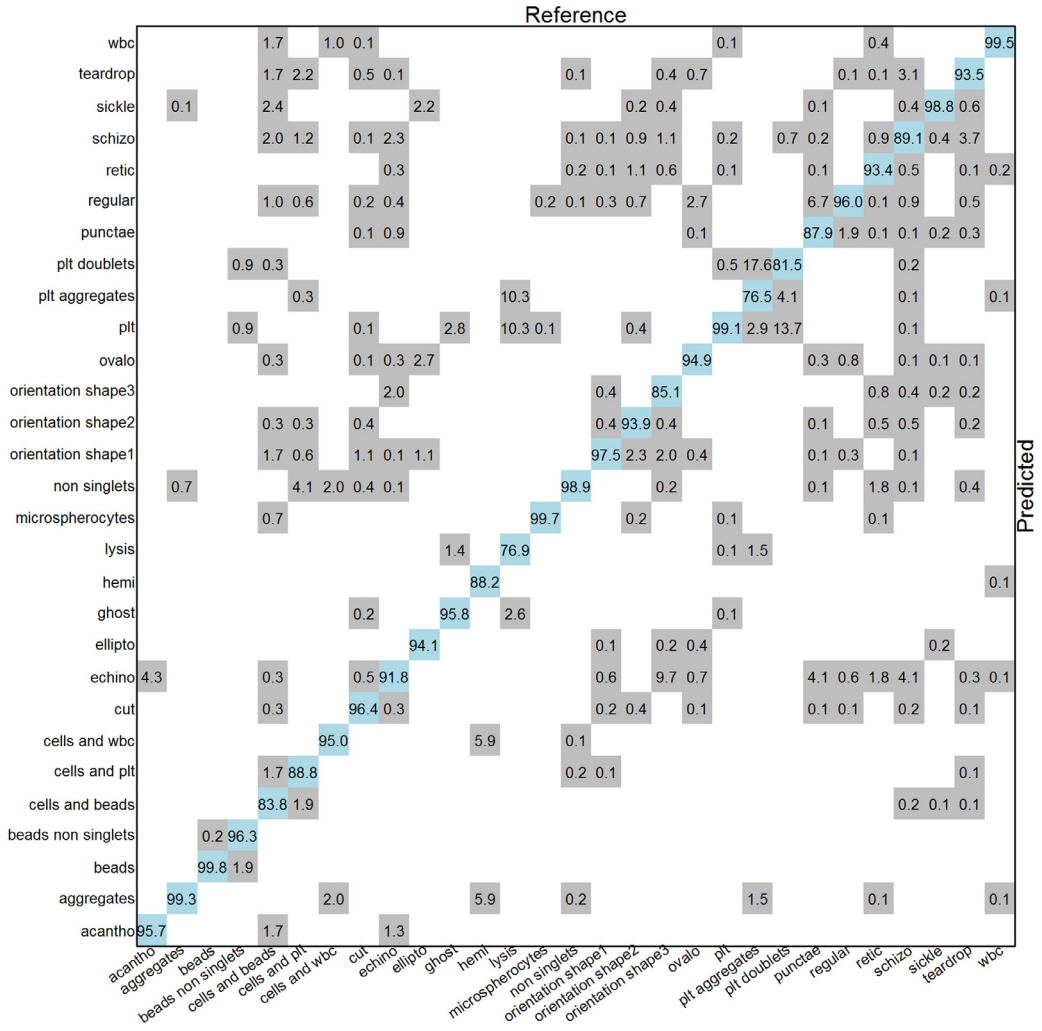

Figure 4. Confusion matrix of reference (manually identified classes) versus predicted (AI attributed classes) percentages after modelling. The rows indicate the predicted classes and the columns the reference classes corresponding to the modelling using the ideas plus keras features. Each blue square represents the percentage of well-classified events. The grey squares represent the percentage of misclassified events.

median CV = 22.1% [11.8–31.9] for samples > 1% schistocytes). We validated the linearity of IFC schistocyte quantification by selecting a sample with a high percentage of schistocytes (4.29% by OM and 7.05% by IFC) and performing serial dilutions in a control sample with no schistocytes. We observed excellent linearity (R^2: 0.98, Suppl. Figure S6). Finally, the median acquisition time was under 30 seconds (median: 20 sec [17-25]) and the SVM categorisation under 3 minutes.

Clinical significance of schistocyte detection by imaging flow cytometry

Given the high positive predictive value of the 1% cut-off for the diagnosis of TMA, we focused on samples with 1% or more schistocytes as determined on blood smears by morphological examination.[7,8] We defined the corresponding cut-off using IFC-based schistocyte quantification by performing receiver operating characteristic (ROC) curve analysis to assess the ability of IFC to identify such samples. The resulting area under the curve (AUC) was 0.993 (CI: 0.983-1.000) (Figure 7a). At a cut-off of 1.92, corresponding to 1% schistocyte count by OM, we obtained a specificity of 91.3% (CI: 82.0-96.7%), a sensitivity of 100.0% (CI: 89.4-100.0%), a negative predictive value (NPV) of 100.0% (CI: 94.3-100.0%), and a positive predictive value (PPV) of 84.6% (CI: 69.5-94.1%), avoiding any risk of missing a TMA diagnosis (effect of prevalence on the predictive values showed in Suppl. Table S7). Of note, 6 samples were detected above this cut-off by IFC whereas they were < 1% on blood smears (0.99%, 0.88%, 0.56%, 0.39%,

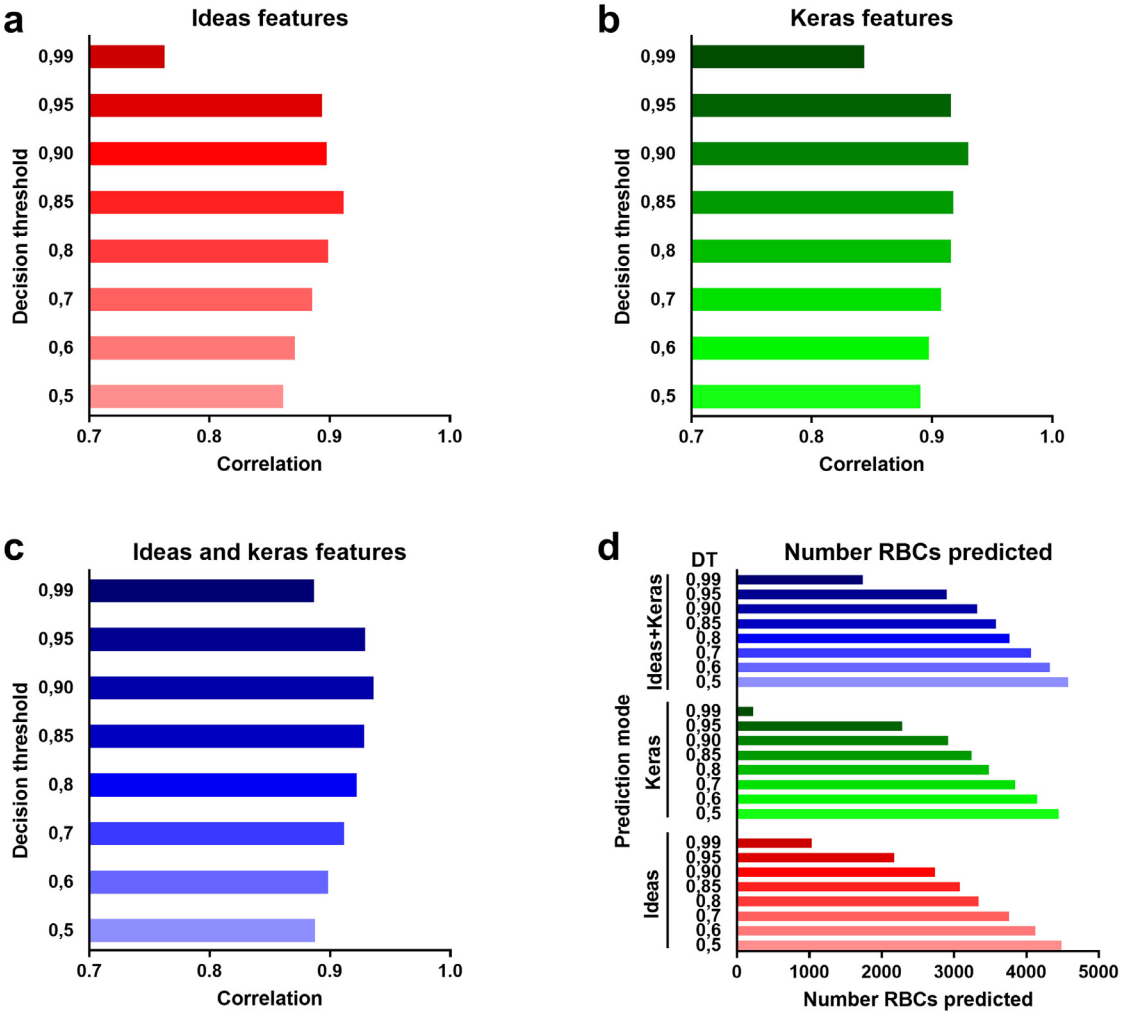

Figure 5. Effect of the decision threshold on the correlation between schistocyte count by IFC and OM and the RBCs counted. (a) Spearman's rank correlation coefficient between mean schistocyte counts and the percentage of IS schistocytes predicted using ideas features alone (*n*=102), (b) keras features alone (*n*=102), (c) ideas and keras features together (*n*=102). (d) Number of remaining RBCs after the application of the decision threshold for the three prediction modes (*n*=102). DT: decision threshold.

0.37, and 0.12%) but no patients with a high probability of TMA by cytology were below the cut-off using IFC (Figure 7b, Suppl. Table S8). We sequentially determined the percentage of schistocytes for five patients for whom successive samples were available using both techniques and observed close patterns over time (Suppl. Figure S7), showing that IFC is accurate not only in identifying schistocytes at diagnosis but also during patient follow-up.

External validation cohort

We independently validated our method on patients recruited in an external healthcare centre. Patients of this cohort are younger (13 years [7-48] *vs* 43 years [30-64]) than the previous cohort and HUS was the predominant aetiology (27/28 samples with schistocytosis *vs* 10/33 samples with schistocytosis). Among a total of 74 samples collected and acquired at Necker Hospital, we obtained a sensitivity of 100% (CI: 88.1-100.0%) and a specificity of 91.1 (CI: 78.8-97.5%) (4 false positive) to detect samples with more than 1% schistocytes. The AUC of the ROC curve was 0.995 (CI: 0.987-1.000) (Figure 7c and d, Suppl. Table S8). The linear regression between schistocyte count by IFC and cytology was Y=1.029x with a correlation of 0.86 (CI: 0.71-0.93) (Suppl. Figure S8). The discrepancy of linear regression between the 2 centres (1.92 in Amiens, Figure 6) can be explained by (i) a lack of standardisation of the schistocyte count by OM between the 2 centres (ii) a non-transposability of our modelling to another instrument. To further investigate those

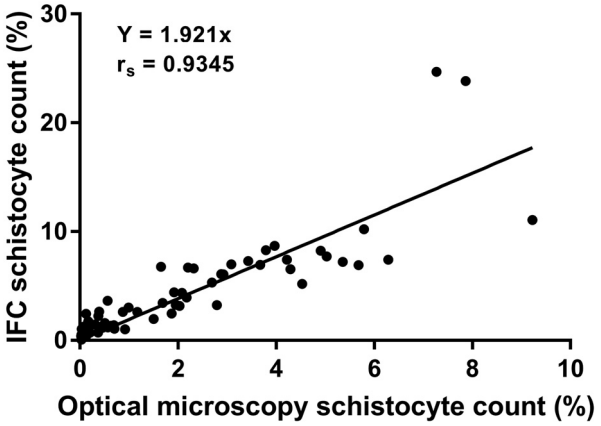

Figure 6. Evaluation of the prediction model using ideas plus keras features with a DT of 0.9 on CBCs for which a schistocyte count was requested. Correlation between mean optical microscopy schistocyte counts and IFC schistocyte counts (n=102). r_s: spearman's rank correlation coefficient. Y: slope of the linear regression. IFC: imaging flow cytometry.

hypotheses, (i) we compared schistocyte counts by optical microscopy between both centres on 7 identical blood smears. The laboratory medical staff from Necker hospital counted 2.05 (CI: 1.3-2.8) fold more schistocytes than observer1 from Amiens Hospital suggesting a lack of observer standardisation between centres (Suppl. Table S9), (ii) we prepared 16 samples with various schistocytes counts from 4 positive samples diluted with healthy patient blood. We acquired simultaneously the samples in the 2 centres and found a perfect correlation between the 2 IFC counts (Y=1.001x) indicating that our modelling can be transposed to the other IFCs (Suppl. Figure S9).

Discussion

An optimal tool for schistocyte quantification must satisfy several criteria: (i) it must identify schistocytes in a heterogeneous RBC population, (ii) it should be a high-throughput technology for high sensitivity, (iii) it should avoid operator bias and any cause of high inter-observer variability, (iv) it should ideally induce no shape modification by pre-analytical processing, (v) it should be rapid, (vi) it should be reproducible between diagnosis centres and (vii) it should respond to ecological and economic considerations, including label-free solutions, the smallest number of reagents, and the lowest amount of waste possible. Various automated tools have been developed over the years but none of them fulfil all these criteria. In the early 2000s, fragmented red cell (FRC) flag was developed to detect schistocytes during blood counting on automated analysers.[34,35] FRC flag offers many advantages, such as the absence of a pre-analytical procedure and its high input and fully automated nature. However, FRC flag showed insufficient performance, which can be explained by the fact that this parameter is based on indirect factors, such as size and the refractory index, but not RBC morphology, and by interference due to various haematological conditions, such as hypochromia,[36] macrocytosis,[7] and thrombocytosis.[37] Automated blood-smear analysis using a digital camera is now routinely used for WBC recognition in the haematology laboratory, but still requires operator-based reclassification of RBC shapes to provide accurate schistocyte quantification.[14] Moreover, its performance depends on the quality of the smear to adequately choose the correct reading area with the proper repartition of cells.[7,8,15,38,39]

By combining the advantages of flow cytometry and microscopy, IFC is a highly suitable technology for RBC evaluation. Indeed, it is a high throughput technology capable of acquiring up to a thousand events per second. Thus, time is not a limiting factor and the precise quantification of rare events is possible.[40] The 60x objective provides a 0.33 µm per pixel resolution brightfield image for each event, permitting its morphological identification.[41] Inherently, both biconcave and abnormal RBC shapes present themselves in spatial positions that differ from those obtained using blood smears, requiring an initial and challenging learning phase, because some RBC shapes can obviously be indiscernible from others depending on their orientation with respect to the camera. Thus, the constitution of the database was a major challenge of our project because of the time it required and the difficulty to tag a large number of images, especially for rare RBC anomalies. However, now that it has been created and validated, this represents the largest database described so far, including more than 135,000 images. We believe that there are opportunities to improve it, with the continuous incorporation of new elements, and to share it between laboratories improving the standardisation of RBC morphology quantification, as required by the ICSH.[7,8] We used a machine learning strategy based on SVM, with inputs coming from ideas and keras features. It is worth noting that there are many other machine-

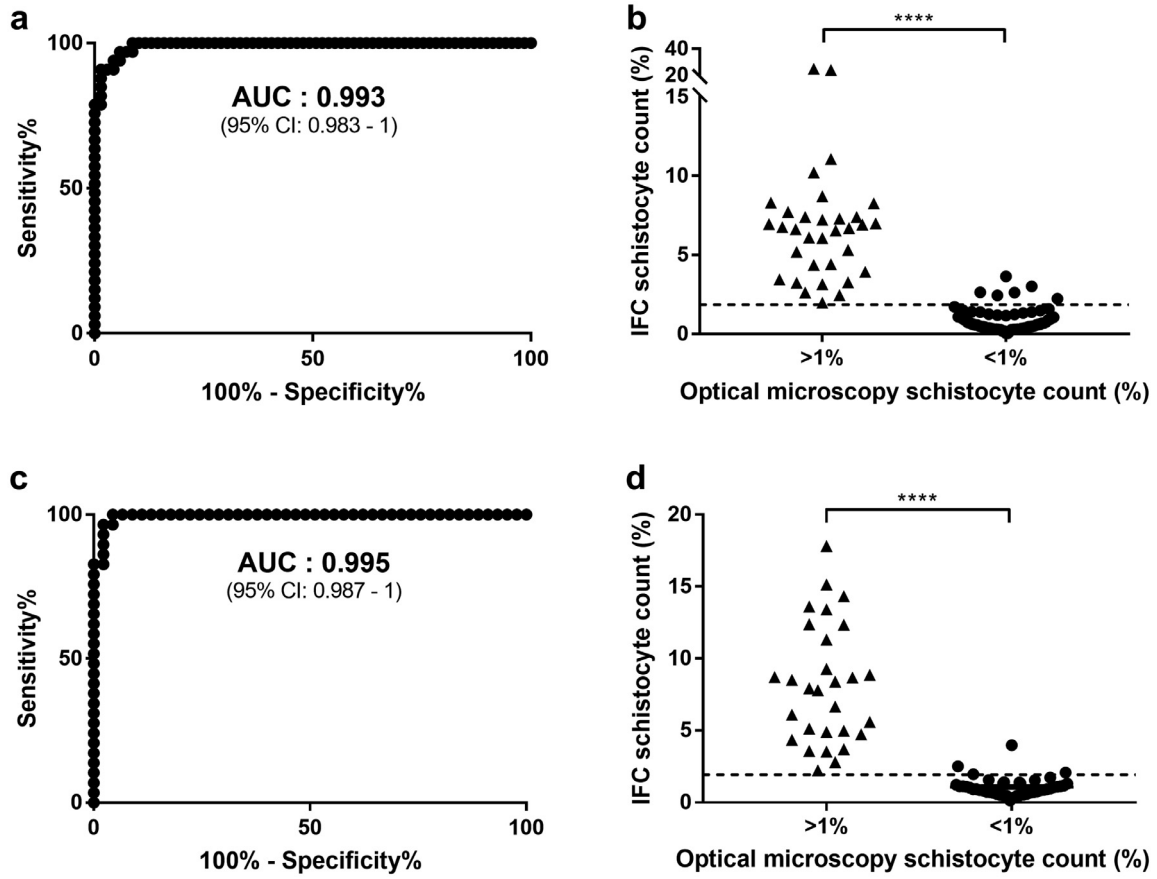

Figure 7. Performance of IFC to detect CBCs with more than 1% schistocytes on blood smears. ROC curve (*n*=102, AUC: 0.993, CI: 0.983 - 1) (a) and bee-swarm plot (b) between patients with > 1% schistocytes (triangle shape, *n*=33, median: 6.68% [4.15-7.56%]) on blood smears and patients with < 1% schistocyte (circle shape, *n*=69, median: 0.61% [0.35-1.13%]) on blood smears from Amiens hospital. ROC curve (*n*=74, AUC: 0.995, CI: 0.987 - 1) (c) and bee-swarm plot (d) between patients with > 1% schistocytes (triangle shape, *n*=29, median: 7.93% [4.81-11.83%]) on blood smears and patients with < 1% schistocyte (circle shape, *n*=45, median: 0.93% [0.68-1.32%]) on blood smears from Necker hospital. The dotted line indicates the cut-off for targeting patients with > 1% schistocytes on blood smear from the others. AUC: area under the curve. ****$p < 0.001$ (Mann-Whitney test). IFC: imaging flow cytometry.

learning algorithms available. For example, Nassar *et* al. evaluated AdaBoost, gradient boosting (GB), K−nearest neighbors (KNN), random forest (RF), and a support vector machine for the classification of WBCs using IFC.[24] Although we applied SVM optimisation, future studies could be conducted to optimise the modelling using these other algorithms and their corresponding hyperparameters. Nonetheless, by combining ideas and keras features, we obtained very high overall accuracy (95.64%, CI: 95.39-95.88) with the validation set. Indeed, we evaluated the use of ideas features, keras features, and the combination of both. Interestingly, keras features provided better results than ideas features whereas the combination of both gave best results. As a consequence, although the development of dedicated masks and the extraction of ad hoc features have shown to be of great interest, it looks highly appealing, as pointed by others, to think that the high information content of IFC images can be adequately captured by deep learning methods to expose disease states.[42–44] With this in mind, our database may provide opportunities for further investigation of this point. Notably, the very simple CNN architecture, which allowed us to quickly train 243,750 parameters to finally extract 128 features on brightfield images on a relatively affordable GPU, may be enriched by more complex topology and additional layers. On the other hand, although the method of combining ideas and keras features was original, it may also be tempting to directly assess the CNN prediction without the feature extraction or final SVM training step we used. Such strategies have been used with success by others using much larger CNNs, such as deepometry software from the Broad Institute, based on ResNet50, or the VGG16 based CNN component of the new Amnis® AI SW package.[25,45]

The schistocyte percentage values obtained by OM and IFC were not the same, with IFC detecting an approximately two-fold higher percentage. This apparent discrepancy is due to (i) the exclusion of RBCs in the side-view category, which represents up to 30% of all events, whereas this category does not exist in OM, and (ii) the application of a decision threshold that restricted the quantification to images with a probability of being correctly classified. Of note, there was a strong correlation between the IFC and OM values, which remained strong during the follow-up of the five TMA patients for whom this data was available. This difference was not found with the external validation cohort despite a perfect correlation of schistocyte counts by IFC between both centres. Our results showed that it was related to the already described inter-observer variability of the schistocyte count by OM highlighting the importance of schistocyte count standardisation.[46,47] Finally, in addition to use as less as 10 µL of blood, IFC was also time saving, with an acquisition time of < 30 s, providing a quantification based on $> 3{,}000$ identified RBCs in less than 3 minutes, and showed excellent repeatability. Overall, these properties compare favourably to the state-of-the-art of schistocyte quantification by cytology. However, our study shows some limitations: (i) the results were determined on a relatively modest sample size in two centres, (ii) samples were not collected consecutively in a prospective manner and (iii) the prevalence of positive samples is biased by their over-representation relative to the general population. Further investigations in a prospective study should allow providing more insights on advanced metrics like sensitivity, specificity, NPV, and PPV in a representative routine clinical population.

Our data strengthen the use of IFC as a promising tool for cell recognition in haematology. Previous reports included masking procedures and/or pre analytical modifications and/or labelling with a regular IFC gating strategy to identify a specific RBC shape. Indeed, sickle cells have been identified after deoxygenation and fixation,[16] whereas certain RBC membrane disorders required EMA staining[20] and intra-erythrocyte inclusions were identified as the four malaria parasite blood stages after fluorescent labelling.[17] Here, we developed a label-free image-based machine learning strategy on human whole blood capable of identifying schistocytes, as well as 13 other categories, such as sickle cells or teardrop cells. Thus, our approach of combining AI and IFC could represent a potentially powerful, rapid, and high input tool for the evaluation of most clinically relevant RBC shapes, although it would require a samples validation step for each, as we performed here for schistocytes. AI-based analysis of cell, tissue, and organ images has seen unprecedented growth in recent years in the field of diagnosis and has been widely validated for the diagnosis of dermatological, ophthalmological, and radiological pathologies, with performance equal to that of humans.[48–50] In malignant haematology, there is growing evidence favouring the use of AI in diagnosis, risk stratification, and treatment options, as described in a recent review.[33] Several studies have underlined the performance of AI in analysing images from peripheral smears for leukocyte recognition.[51] Others focused on RBCs shape identification, but were based only on selected and tagged images (test set) or on a limited number of blood samples.[52,53] Using IFC in association with AI is pushing the limits of cell recognition in haematological cytology. Doan et *al.* observed that T and B lymphocytes can be morphologically recognised by IFC and AI while they are indistinguishable to the human eye on a blood smear.[24] Zhou et *al.* classified platelet aggregates generated *in vitro* according to the activating agonist using the same strategy.[54] Nishikawa et al. used AI and IFC to investigate platelet aggregates levels in COVID-19 patients.[55] These proofs of concept show that AI can detect morphological features that are imperceptible by humans. Focusing on RBCs, Doan et *al.* recently generated a database of 67,400 cells that could recognise six morphologies corresponding to different steps in the *in vitro* aging of stored RBCs.[26] Our results have been settled in one healthcare centre and confirmed in one another, both equipped with different instruments, yet providing similar results, emphasising that such recent approaches to further put IFC and AI into clinics offer highly valuable results in deep learning workflows.[26,27]

Contributors

J.D., M.L.G., E.G., V.H., T.B., C.R., and M. Dussiot, participated in data and samples collection; J.D., M.L.G., and L.G. counted the blood smears; Y.D. performed the bioinformatics analysis; J.D. and M. Diouf performed statistical analysis; Y.D., J.D., E.G., C.R., and M. Dussiot acquired blood samples; J.D., Y.D., and L.G. wrote the paper; All authors have read and approved the final manuscript. J.D. and C.R. have verified the underlying data.

Data sharing statement

De-identified Case and Control values with all statistical analysis will be made available. Models created in this study will be available from corresponding authors. A list of software used for this study and notably the IFC package used for features extraction is provided in Suppl. Table S4 including links to version controlled where it applies.

Declaration of interests

All authors declare that they have no conflicts of interest.

Acknowledgements

None.

Supplementary materials

Supplementary material associated with this article can be found in the online version at doi:10.1016/j.ebiom.2022.104209.

References

1 Palmer L, Briggs C, McFadden S, et al. ICSH recommendations for the standardization of nomenclature and grading of peripheral blood cell morphological features. *Int J Lab Hematol*. 2015;37(3):287–303.
2 Ahmed M, Patel AR. Evaluation of normal reference range of schistocytes and burr cells in healthy adults. *Blood*. 2015;126(23):4540.
3 Burns ER, Lou Y, Pathak A. Morphologic diagnosis of thrombotic thrombocytopenic purpura. *Am J Hematol*. 2004;75(1):18–21.
4 Bain BJ, Bates I, Laffan MA, Lewis SM. *Dacie and Lewis practical haematology*. 12th ed. Elsevier; 2017.
5 Joly BS, Coppo P, Veyradier A. Thrombotic thrombocytopenic purpura. *Blood*. 2017;129(21):2836–2846.
6 George JN, Nester CM. Syndromes of thrombotic microangiopathy. *N Engl J Med*. 2014;371(7):654–666.
7 Zini G, d'Onofrio G, Briggs C, et al. ICSH recommendations for identification, diagnostic value, and quantitation of schistocytes. *Int J Lab Hematol*. 2012;34(2):107–116.
8 Zini G, d'Onofrio G, Erber WN, et al. 2021 Update of the 2012 ICSH recommendations for identification, diagnostic value, and quantitation of schistocytes: impact and revisions. *Int J Lab Hematol*. 2021;43(6):1264–1271.
9 George JN. TTP: the evolution of clinical practice. *Blood*. 2021;137(6):719–720.
10 Rümke CL. The imprecision of the ratio of two percentages observed in differential white blood cell counts: a warning. *Blood Cells*. 1985;11(1):137–140.
11 Kratz A, Lee S, Zini G, et al. Digital morphology analyzers in hematology: ICSH review and recommendations. *Int J Lab Hematol*. 2019;41(4):437–447.
12 Kim HN, Hur M, Kim H, Kim SW, Moon HW, Yun YM. Performance of automated digital cell imaging analyzer Sysmex DI-60. *Clin Chem Lab Med CCLM*. 2017;56(1):94–102.
13 Criel M, Godefroid M, Deckers B, Devos H, Cauwelier B, Emmerechts J. Evaluation of the red blood cell advanced software application on the CellaVision DM96. *Int J Lab Hematol*. 2016;38(4):366–374.
14 Hervent AS, Godefroid M, Cauwelier B, Billiet J, Emmerechts J. Evaluation of schistocyte analysis by a novel automated digital cell morphology application. *Int J Lab Hematol*. 2015;37(5):588–596.
15 Saad Albichr I, Sottiaux J, Hotton J, De Laveleye M, Dupret P, Detry G. Cross-evaluation of five slidemakers and three automated image analysis systems: the pitfalls of automation? *Int J Lab Hematol*. 2020;42(5):573–580.
16 van Beers EJ, Samsel L, Mendelsohn L, et al. Imaging flow cytometry for automated detection of hypoxia-induced erythrocyte shape change in sickle cell disease: SIFCA for automated detection of hypoxia-induced sickling. *Am J Hematol*. 2014;89(6):598–603.
17 Dekel E, Rivkin A, Heidenreich M, et al. Identification and classification of the malaria parasite blood developmental stages, using imaging flow cytometry. *Methods*. 2017;112:157–166.
18 Roussel C, Morel A, Dussiot M, et al. Rapid clearance of storage-induced microerythrocytes alters transfusion recovery. *Blood*. 2021;137(17):2285–2298.
19 Roussel C, Dussiot M, Marin M, et al. Spherocytic shift of red blood cells during storage provides a quantitative whole cell-based marker of the storage lesion: Spherocytic shift of RBCs during storage. *Transfusion*. 2017;57(4):1007–1018.
20 More TA, Dalal B, Devendra R, Warang P, Shankarkumar A, Kedar P. Applications of imaging flow cytometry in the diagnostic assessment of red cell membrane disorders. *Cytometry B Clin Cytom*. 2020;98(3):238–249.
21 Dominical V, Samsel L, McCoy JP. Masks in imaging flow cytometry. *Methods*. 2017;112:9–17.
22 Filby A, Houston JP. Imaging cytometry: automated morphology and feature extraction: editorial. *Cytometry A*. 2017;91(9):851–853.
23 Lippeveld M, Knill C, Ladlow E, et al. Classification of human white blood cells using machine learning for stain-free imaging flow cytometry. *Cytometry A*. 2020;97(3):308–319.
24 Nassar M, Doan M, Filby A, et al. Label-free identification of white blood cells using machine learning. *Cytometry A*. 2019;95(8):836–842.
25 Doan M, Case M, Masic D, et al. Label-free leukemia monitoring by computer vision. *Cytometry A*. 2020;97(4):407–414.
26 Doan M, Sebastian JA, Caicedo JC, et al. Objective assessment of stored blood quality by deep learning. *Proc Natl Acad Sci*. 2020;117(35):21381–21390.
27 Wills JW, Verma JR, Rees BJ, et al. Inter-laboratory automation of the in vitro micronucleus assay using imaging flow cytometry and deep learning. *Arch Toxicol*. 2021;95(9):3101–3115.
28 Ghosh S, Dasgupta A, Swetapadma A. A study on support vector machine based linear and non-linear pattern classification. *2019 International Conference on Intelligent Sustainable Systems (ICISS)*. Palladam, Tamilnadu, India: IEEE; 2019:24–28. [cited 2022 Jul 6] Available from: https://ieeexplore.ieee.org/document/8908018/.
29 Koo TK, Li MY. A guideline of selecting and reporting intraclass correlation coefficients for reliability research. *J Chiropr Med*. 2016;15(2):155–163.
30 Shrout PE, Fleiss JL. Intraclass correlations: uses in assessing rater reliability. *Psychol Bull*. 1979;86(2):420–428.
31 Lesesve JF, Salignac S, Lecompte T, on behalf of the Groupe Français d'Hématologie Cellulaire. Spherocytes, irregularly contracted cells or ... schistocytes? *Clin Lab Haematol*. 2002;24(2):135–136.
32 Shouval R, Fein JA, Savani B, Mohty M, Nagler A. Machine learning and artificial intelligence in haematology. *Br J Haematol*. 2021;192(2):239–250.
33 Radakovich N, Nagy M, Nazha A. Machine learning in haematological malignancies. *Lancet Haematol*. 2020;7(7):e541–e550.
34 Kunicka JE, Fischer G, Murphy J, Zelmanovic D. Improved platelet counting using two-dimensional laser light scatter. *Am J Clin Pathol*. 2000;114(2):283–289.
35 Jiang M, Saigo K, Kumagai S, et al. Quantification of red blood cell fragmentation by automated haematology analyser XE-2100. *Clin Lab Haematol*. 2001;23(3):167–172.
36 Chalvatzi K, Spiroglou S, Nikolaidou A, Diza E. Evaluation of fragmented red cell (FRC) counting using Sysmex XE-5000 - does hypochromia play a role? *Int J Lab Hematol*. 2013;35(2):193–199.
37 Lesesve JF, Asnafi V, Braun F, Zini G. Fragmented red blood cells automated measurement is a useful parameter to exclude schistocytes on the blood film. *Int J Lab Hematol*. 2012;34(6):566–576.
38 Billard M, Lainey E, Armoogum P, Alberti C, Fenneteau O, Da Costa L. Original article: evaluation of the CellaVision™ DM automated microscope in pediatrics. *Int J Lab Hematol*. 2010;32(5):530–538.
39 Park SJ, Yoon J, Kwon JA, Yoon SY. Evaluation of the CellaVision advanced RBC application for detecting red blood cell morphological abnormalities. *Ann Lab Med*. 2021;41(1):44–50.
40 Ogle LF, Orr JG, Willoughby CE, et al. Imagestream detection and characterisation of circulating tumour cells – a liquid biopsy for hepatocellular carcinoma? *J Hepatol*. 2016;65(2):305–313.
41 Voronin DV, Kozlova AA, Verkhovskii RA, et al. Detection of rare objects by flow cytometry: imaging, cell sorting, and deep learning approaches. *Int J Mol Sci*. 2020;21(7):2323.
42 Filby A, Davies D. Reporting imaging flow cytometry data for publication: why mask the detail? *Cytometry A*. 2012;81A(8):637–642.
43 Doan M, Vorobjev I, Rees P, et al. Diagnostic potential of imaging flow cytometry. *Trends Biotechnol*. 2018;36(7):649–652.
44 Shifat-E-Rabbi M, Yin X, Fitzgerald CE, Rohde GK. Cell image classification: a comparative overview. *Cytometry A*. 2020;97(4):347–362.
45 Probst C, Zayats A, Venkatachalam V, Davidson B. Advanced characterization of silicone oil droplets in protein therapeutics using artificial intelligence analysis of imaging flow cytometry data. *J Pharm Sci*. 2020;109(10):2996–3005.
46 Noutsos T, Laidman AY, Survela L, et al. An evaluation of existing manual blood film schistocyte quantitation guidelines and a new proposed method. *Pathology*. 2021;53(6):746–752.
47 Lesesve JF, Lecompte T, Alla F, et al. Reproductibility of the morphological identification of schisocytes and evaluation of non observer-dependent methods. *Ann Biol Clin*. 2005;63(3):279–289.
48 Esteva A, Kuprel B, Novoa RA, et al. Dermatologist-level classification of skin cancer with deep neural networks. *Nature*. 2017;542(7639):115–118.
49 Milea D, Najjar RP, Jiang Z, et al. Artificial Intelligence to detect papilledema from ocular fundus photographs. *N Engl J Med*. 2020;382(18):1687–1695.
50 Hosny A, Parmar C, Quackenbush J, Schwartz LH, Aerts HJWL. Artificial intelligence in radiology. *Nat Rev Cancer*. 2018;18(8):500–510.

51 Wang Q, Bi S, Sun M, Wang Y, Wang D, Yang S. Deep learning approach to peripheral leukocyte recognition. Zhang J, editor. *PLoS One*. 2019;14(6):e0218808.

52 Durant TJS, Olson EM, Schulz WL, Torres R. Very deep convolutional neural networks for morphologic classification of erythrocytes. *Clin Chem*. 2017;63(12):1847–1855.

53 Simionato G, Hinkelmann K, Chachanidze R, et al. Red blood cell phenotyping from 3D confocal images using artificial neural networks. Schneidman-Duhovny D, editor. *PLoS Comput Biol*. 2021;17(5):e1008934.

54 Zhou Y, Yasumoto A, Lei C, et al. Intelligent classification of platelet aggregates by agonist type. *eLife*. 2020;9:e52938.

55 Nishikawa M, Kanno H, Zhou Y, et al. Massive image-based single-cell profiling reveals high levels of circulating platelet aggregates in patients with COVID-19. *Nat Commun*. 2021;12(1):7135.